JACS
JOURNAL OF THE AMERICAN CHEMICAL SOCIETY
pubs.acs.org/JACS
Article

Thermally Controlled Exciplex Fluorescence in a Dynamic Homo[2]catenane

Amine Garci,[○] Arthur H. G. David,[○] Laura Le Bras, Marco Ovalle, Seifallah Abid, Ryan M. Young, Wenqi Liu, Chandra S. Azad, Paige J. Brown, Michael R Wasielewski, and J. Fraser Stoddart*

Cite This: J. Am. Chem. Soc. 2022, 144, 23551−23559
Read Online
ACCESS | Metrics & More | Article Recommendations | Supporting Information

ABSTRACT: Motion-induced change in emission (MICE) is a phenomenon that can be employed to develop various types of probes, including temperature and viscosity sensors. Although MICE, arising from the conformational motion in particular compounds, has been studied extensively, this phenomenon has not been investigated in depth in mechanically interlocked molecules (MIMs) undergoing coconformational changes. Herein, we report the investigation of a thermoresponsive dynamic homo[2]catenane incorporating pyrene units and displaying relative circumrotational motions of its cyclophanes as evidenced by variable-temperature ^{1}H NMR spectroscopy and supported by its visualization through molecular dynamics simulations and quantum mechanics calculations. The relative coconformational motions induce a significant change in the fluorescence emission of the homo[2]catenane upon changes in temperature compared with its component cyclophanes. This variation in the exciplex emission of the homo[2]catenane is reversible as demonstrated by four complete cooling and heating cycles. This research opens up possibilities of using the coconformational changes in MIMs-based chromophores for probing fluctuations in temperature which could lead to applications in biomedicine or materials science.

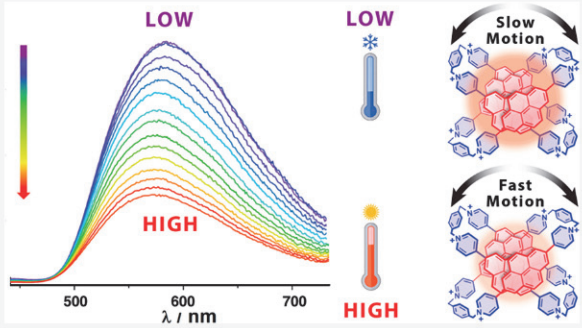

INTRODUCTION

Temperature is a physical effect brought about by the thermal agitation of particles. For centuries, its measurement[1] has been of major importance in numerous contexts, particularly in biomedicine,[2] meteorology,[3] and industry.[4] The development of luminescent molecular probes[5] capable of sensing temperature in nano- and microenvironments has increased[6] considerably during the past 20 years. Some of these sensors rely on a motion-induced change in emission[7] (MICE) in which conformational changes in molecules can be modulated,[8] resulting in the modification of their luminescence. Thus, when the relative movements of these fluorophores are constrained, their emission is favored, and when they are allowed, nonradiative relaxations dominate, causing a decrease in fluorescence.

Catenanes[9] are a class of mechanically interlocked molecules[10] (MIMs) composed of two or more interlocked rings linked by one or more mechanical bonds. Over the years, fluorescent catenanes have been developed[11] and found diverse applications, ranging from sensing[12] to bioimaging.[13] Recently, we have designed[14] a series of emissive tetracationic cyclophanes[15] and discovered that some of these cyclophanes incorporating anthracene,[13] pyrene,[16] and diazaperopyrenium[17] units can participate in the formation of homo[2]catenanes. Remarkably, the nanoconfinement of these fluorophores, on account of mechanical bonding in homo[2]catenanes, induces[13,16] a permanent exciplex emission. Consequently, the anthracene-based homo[2]catenane was employed[13] in live cell imaging, while the pyrene-based homo[2]catenane analogs were used[16] as photocatalysts.

Furthermore, catenanes have shown[18] relevant temperature-controlled behavior on account of the relative coconformational motions undergone by their mechanically interlocked rings. Although the dynamics of thermoresponsive catenanes have been explored[18] mainly by variable-temperature (VT) ^{1}H NMR spectroscopy, their changes in fluorescence, on account of the temperature-induced coconformational dependent motion, remain underexplored.[19,20] In this context, the investigation of the relationship between temperature-controlled movement and the fluorescence of emissive homo[2]catenanes is of fundamental importance.

Herein, we describe the effect of temperature on the relative coconformational changes and the exciplex emission (Figure 1) of the pyrene-based homo[2]catenane,[16] e.g., $^{2,7-2,7}$**PyHC**$^{8+}$. A combination of VT ^{1}H NMR, UV−vis absorption, and emission spectroscopies, as well as molecular dynamics (MD) and

Received: October 6, 2022
Published: December 13, 2022

https://doi.org/10.1021/jacs.2c10591
J. Am. Chem. Soc. 2022, 144, 23551−23559

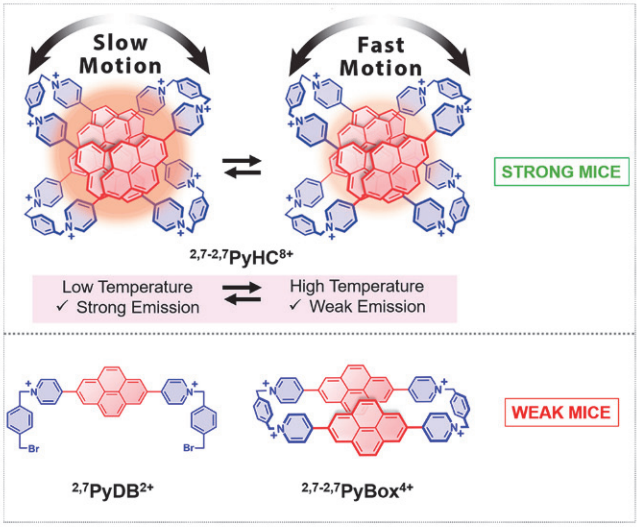

Figure 1. Structural formulas of $^{2,7-2,7}$**PyHC**$^{8+}$, ^{2,7}**PyDB**$^{2+}$, and $^{2,7-2,7}$**PyBox**$^{4+}$. The homo[2]catenane exhibits strong MICE. At high temperature, the relative coconformational motion of the two identical rings in the homo[2]catenane is fast, leading to a decrease in the exciplex-emission intensity, while, at low temperature, this motion is slower, resulting in a higher fluorescence intensity. Conversely, in the case of the monomeric-emissive ^{2,7}**PyDB**$^{2+}$ and $^{2,7-2,7}$**PyBox**$^{4+}$, the absence of the mechanical bonds and coconformational motions of the rings produce a weak MICE arising from their conformational changes.

quantum mechanics (QM) calculations, have been employed to understand and explain the effect of these relative coconformational changes on the exciplex emission of the catenane.

EXPERIMENTAL SECTION

Molecular Dynamics. Molecular dynamics (MD) simulations were run within the GROMACS 2018.3 package.[21] $^{2,7-2,7}$**PyHC**$^{8+}$ and water (TIP3P) molecules were described using the generalized AMBER force field[22] (GAFF). As GAFF is not directly implemented in GROMACS, acpypi script[23] was used to convert the files from AMBER to GROMACS formalism. For the $^{2,7-2,7}$**PyHC**$^{8+}$ molecule, atomic charges were derived following the parametrization procedure in GAFF based on HF-6-31G(d) RESP charges. In order to render the system neutral during the simulation, 8 chloride anions were added within the solvent molecules. The simulation box is a 60 × 60 × 60 Å^3 filled with one $^{2,7-2,7}$**PyHC**$^{8+}$, 8 chloride anions, and approximatively 7500 H_2O molecules. In order to observe and characterize coconformational motion, constraints were applied on one of the two rings of $^{2,7-2,7}$**PyHC**$^{8+}$ during the simulation.

Periodic boundary conditions were imposed to describe the electrostatic interactions, along with a cutoff of 10 Å and the use of the Particle Mesh Ewald method.[24] After a minimization step using the steepest descents method, two consecutive equilibration steps were performed. A simulation in the canonical ensemble (NVT) during 1000 ps was first of all carried out. The temperature—either 293 or 343 K—was set using the Berendsen weak coupling method.[25] Nonsolvent (^{2,7}**PyHC**$^{8+}$ and anions) and solvent molecules were coupled to separate temperature coupling baths. Then, a simulation under constant pressure (NPT) was undertaken for again 1000 ps. The isobaric character of the simulation (P = 1 bar) is ensured using the previously mentioned weak-coupling Berendsen method. The production phase was then carried out in the same NPT ensemble with a time step of 2 fs. The temperature and pressure were maintained using a Nosé−Hoover thermostat[26] (τ = 1 ps) and Parinello−Rahman barostat[27] (τ = 1 ps), respectively. The simulation time was set to 50 ns.

Quantum Mechanics. Single-point energy calculations were performed using a Gaussian09 package[28] within the density functional theory (DFT) framework. The ωB97X-D range separated hybrid exchange correlation functional (XCF) was used in combination with the 6-311+G(d,p) atomic basis set.[29] This XCF has already proven its efficiency when dealing with supramolecular interactions.[30] The solvent (H_2O) was represented implicitly with a polarizable continuum model[31] (PCM). The densities that have been calculated at this QM level have been used for noncovalent interactions (NCI) analysis.

For the computation of the energetic barriers (Figure 2d), 20 coconformations have been considered within a rigid scan. Ten of them allow the description of the translational movement, and the other 10 are accounted for by partial circumrotation. The translational movement corresponds (Figure S2a) to a variation in the distance between the bridging *p*-xylylene units in the two cyclophanes. The partial-circumrotation is characterized by the passage of one cyclophane with respect to the other one (Figure S2b) over the bridging *p*-

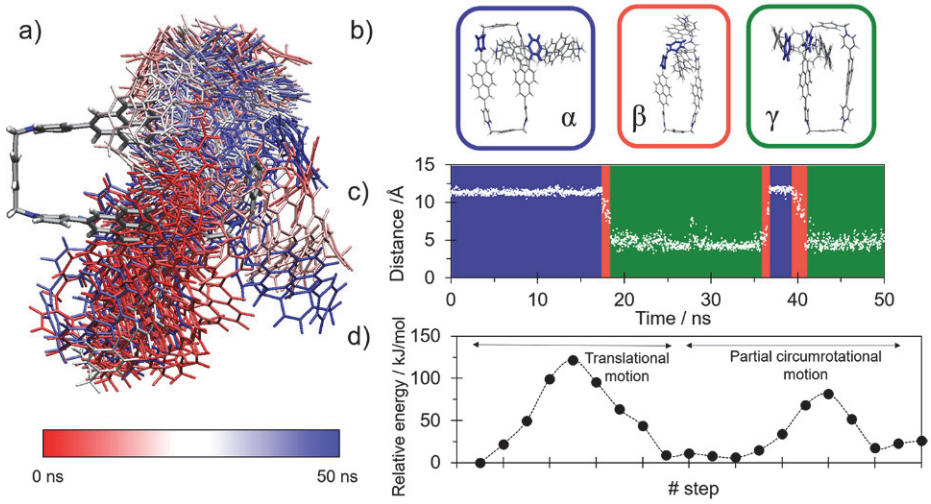

Figure 2. (a) Tubular-and-stick representation along the 50-ns MD simulation of the coconformations of $^{2,7-2,7}$**PyHC**$^{8+}$ at 293 K, displaying the circumrotational movements between the two mechanically interlocked cyclophanes. (b) Stick representation of the three average structures (α, β, and γ) illustrating the circumrotation of one of the rings with respect to the other. In each of the three average structures, one pyridinium unit has been highlighted in blue. (c) The evolution of the distance is recorded, in Å, between the center of mass of the highlighted pyridinium units displayed in Figure 2b. (d) The energy profile, in kJ/mol, for the two components undergoing relative circumrotational motions. See Figure S6 for the step numbers representing 20 coconformations.

https://doi.org/10.1021/jacs.2c10591
J. Am. Chem. Soc. 2022, 144, 23551−23559

xylylene unit. The energy was comuted for each coconformation represented. The most stable coconformation has been assigned zero-point energy, and all the other energies are expressed relative to this reference point.

Noncovalent Interaction Analysis. Noncovalent interactions (NCI) have been visualized with NCIPLOT.[32] The NCI analysis is based on the calculated electronic density and its reduced gradient (s) and can be represented as a two-dimensional plot. When atoms or molecules are interacting, the reduced density gradient goes toward zero and the NCIs can be identified. The reduced-density gradient information on its own, however, does not allow the differentiation of attractive and repulsive interactions. It is necessary to examine the second density Hessian eigenvalue (λ_2) to determine whether the NCIs are attractive or repulsive. To summarize, NCIs are identified at low values of the density-reduced gradient. Those NCIs can be attractive ($\lambda_2 < 0$) or repulsive ($\lambda_2 > 0$). The strengths of the NCIs are obtained by multiplying the sign of λ_2 with the density (ρ). NCIs are defined from strongly attractive to strongly repulsive through van der Waals weak interactions.

UV/vis Absorption and Fluorescence Emission Spectroscopic Analyses. UV/vis absorption and fluorescence emission spectra were recorded on a UV-3600 Shimadzu spectrophotometer and a Horiba scientific Fluoromax-4 spectrofluorometer, respectively. Absorption spectra of $^{2,7-2,7}$**PyHC**$^{8+}$ were recorded in HPLC grade solvents at 25 °C at a concentration ca. 1×10^{-6} M. Variable temperature (VT) absorption spectra of $^{2,7-2,7}$**PyHC**$^{8+}$ and $^{2,7-2,7}$**PyBox**$^{4+}$ were recorded in HPLC grade MeCN at a concentration ca. 1×10^{-6} M. The emission spectra of $^{2,7-2,7}$**PyHC**$^{8+}$, $^{2,7-2,7}$**PyBox**$^{4+}$, and ^{2,7}**PyDB**$^{2+}$ were recorded at *ca.* 5×10^{-7} M in HPLC grade solvents. For fluorescence measurements, a fixed slit-width of 3 nm and 0.1 s of integration time were selected. The reversibility of the changes in fluorescence, dependent on the temperature, was carried out employing a solution of $^{2,7-2,7}$**PyHC**$^{8+}$ at *ca.* 5×10^{-7} M in HPLC grade MeCN. After each change of temperature, the solution was allowed to equilibrate for 10 min before measuring the fluorescence. In order to measure the cryogenic emission, a solution of ^{2,7}**PyHC**·8PF_6 in butyronitrile (^{n}PrCN) with an OD of about 0.2 at 350 nm in a 2-mm cuvette was loaded into a dry quartz tube (Wilmad 707-SQ-250M) with a diameter of 4 mm. The sample was then subjected to four freeze–pump–thaw cycles on a vacuum line (10^{-4} Torr) and sealed with a hydrogen torch. Steady-state emission spectra were collected on a Horiba Nanolog fluorimeter with λ_{ex} = 350 nm and a perpendicular arrangement of the excitation source and detector. Spectra were collected at room temperature and at 77 K by submersing the sealed tube into a liquid nitrogen bath.

Variable-Temperature Transient Absorption Spectroscopic Analyses. Variable-temperature visible nanosecond transient absorption (nsTA) spectroscopy was performed using a previously described apparatus.[33] The 355 nm, ~100 fs pump pulses were generated at 1 μJ per pulse using a commercial collinear optical parametric amplifier (TOPAS-Prime, Light-Conversion, Ltd.). The pump polarization was randomized using a commercial depolarizer (DPU-25-A, Thorlabs, Inc.) to eliminate any orientational dynamics resulting from the experiment. Spectra were collected on a commercial spectrometer (customized EOS, Ultrafast Systems). All samples were stirred to avoid localized heating or degradation effects. The optical density was maintained at 0.6 for all samples. Time-resolved fluorescence spectroscopy was performed on an instrument described previously[33] with 350-nm excitation pulses attenuated to <10 nJ/pulse and sample ODs < 0.1. Sample temperature during experiments was maintained using a thermoelectric cuvette holder (Flash 100) with a temperature controller (Quantum Northwest). Single-wavelength kinetic analysis was performed using a nonlinear least-squares fit to a sum of exponentials convoluted with a Gaussian instrument response function.

RESULTS AND DISCUSSION

The dynamic behavior of the thermostable $^{2,7-2,7}$**PyHC**$^{8+}$ has been investigated previously[16] by ^{1}H NMR spectroscopy in three different solvents—namely, CD_3CN, MeOD, and D_2O. In the present investigation the relative coconformational motions of the cyclophanes in this [2]catenane were investigated in DMF-d_7 by VT ^{1}H NMR spectroscopy. The spectra (Figure S1) show the following responses—(i) Two sets of resonances corresponding to the external and internal (primed) protons are observed at a relatively low temperature; (ii) coalescence which is detected at relatively high temperature where the resonances become broad. The reason for this coalescence is the relative circumrotational motions undergone by the two mechanically interlocked rings, rendering the internal (primed) and external protons indistinguishable on the ^{1}H NMR time scale. Unlike the homo[2]catenane, the cyclophane $^{2,7-2,7}$**PyBox**$^{4+}$, which does not experience coconformational changes, exhibits (Figure S4) ^{1}H NMR spectra independent of temperature, i.e., no changes of chemical shift are observed upon altering the temperature.

Table 1. Summary of the Rate (k) for the Circumrotation of $^{2,7-2,7}$PyHC^{8+} in CD_3CN, MeOD and DMF-d_7 Showing the Increase in Rate Constant k as the Temperature Increases

	k/s^{-1}[a]		
T/K	CD_3CN	MeOD	DMF-d_7
293	5.9	15	1.3
298	8.5	21	2.3
303	12	28	4.1
313	24	49	12
323	46	84	33
333	85	137	84
343	150	220[b]	204

[a]The rate was calculated employing the Eyring equation (Figure S3 and ref 16). [b]This value is extrapolated because it is above the boiling point of the solvent.

Furthermore, the circumrotation rates (k) (Table 1) of $^{2,7-2,7}$**PyHC**$^{8+}$, which have been estimated by ^{1}H NMR line-shape analysis[34] (Figures S2 and S3), reveal that, in CD_3CN, MeOD, and DMF-d_7, the relative motion of the cyclophanes at 293 K is slow, but increases significantly at higher temperature. Remarkably, the acceleration of the rates of circumrotation between 293 and 343 K is much higher in DMF-d_7 wherein k increases 157 times, while it increases only 25.4 and 14.7 times, respectively, in CD_3CN and MeOD.

In order to gain a better understanding of the origin of the dynamic behavior occurring in the homo[2]catenane, the relative coconformational motions of the two cyclophanes in $^{2,7-2,7}$**PyHC**$^{8+}$ have been explored employing a combination of classical MD simulations and QM calculations. NCI analyses have also been used in order to provide a visualization of the interactions within $^{2,7-2,7}$**PyHC**$^{8+}$. For more details about these different computational approaches, see the Experimental Section. MD simulations highlight (Figure 2a, Video S1) rocking and partial but not full circumrotation. The coconformations oscillate (Figure 2b) between two distinct positions, α and γ, involving two pyridinium units on the cyclophane separated by a bridging *p*-xylylene unit. In addition, a less probable intermediate (position β in Figure 2b,c), centered on the bridging *p*-xylylene unit is observed. Noteworthy is the fact that increasing the temperature from 293 to 343 K is followed by an increase in the number of partial circumrotational movements, an observation which is in complete agreement (Figure S5) with the experimental results.

https://doi.org/10.1021/jacs.2c10591
J. Am. Chem. Soc. 2022, 144, 23551−23559

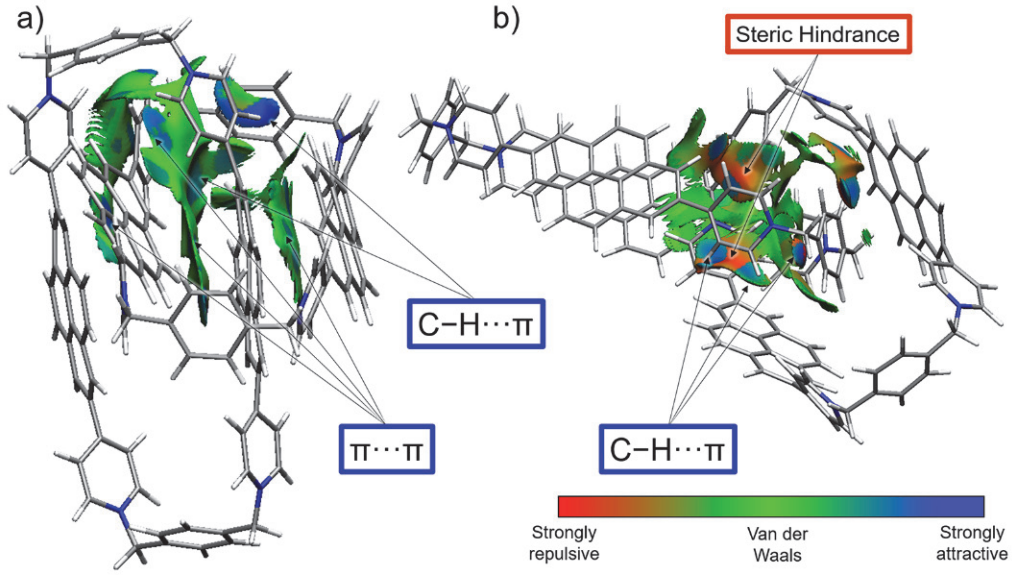

Figure 3. Isosurfaces [$s(r) = 0.4$] for (a) a favorable coconformation (relative energy <10 kJ/mol, Figure 2d) and (b) a less favorable coconformation (relative energy ~70 kJ/mol Figure 2d). Attractive interactions [C–H···π] and [π···π] are depicted in blue, repulsive ones (steric hindrance) in red, and van der Waals interactions in green. Isosurfaces were generated using NCIPLOT.[32b]

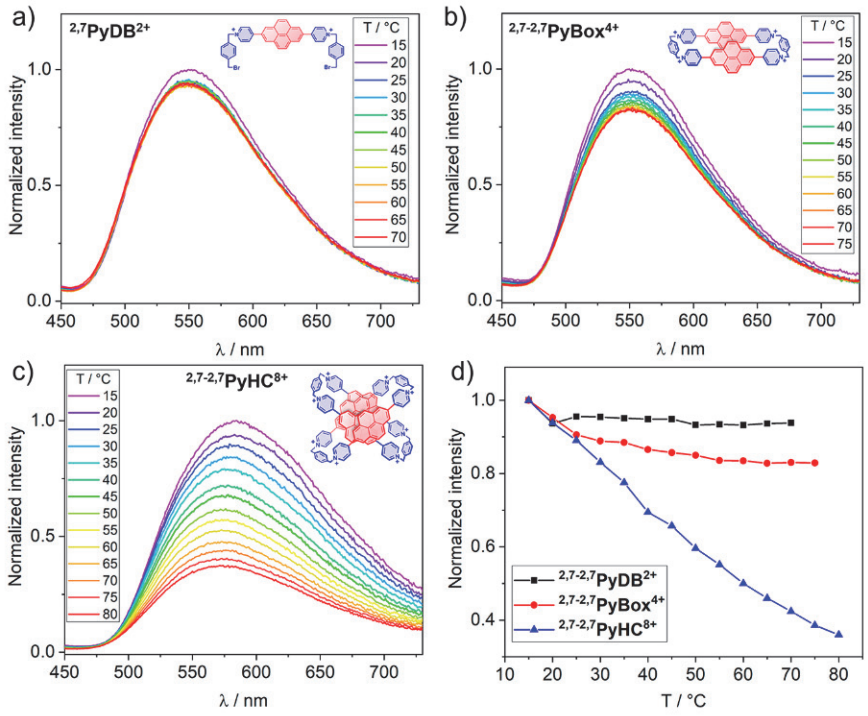

Figure 4. VT emission spectra (λ_{exc} = 376 nm) of (a) ^{2,7}**PyDB**·2PF$_6$, (b) $^{2,7-2,7}$**PyBox**·4PF$_6$, and (c) $^{2,7-2,7}$**PyHC**·8PF$_6$ in MeCN. (d) Graphs showing the performance of the temperature-induced changes in emission for ^{2,7}**PyDB**·2PF$_6$, $^{2,7-2,7}$**PyBox**·4PF$_6$, and $^{2,7-2,7}$**PyHC**·8PF$_6$ in MeCN. These spectra reveal that the changes in emission are much more significant in the homo[2]catenane as a result of the changes in its coconformation with temperature. Furthermore, $^{2,7-2,7}$**PyHC**·8PF$_6$ displays, upon heating, a hypsochromic shift of $\Delta\lambda_{max}$ = 13 nm.

In order to assess the possibility of full circumrotation of one cyclophane with respect to the other, two components of this motion have been identified: (i) a translational movement along the pyrene unit of one cyclophane by the other one, and (ii) partial circumrotation over the bridging *p*-xylylene unit (Figure S6). The energy barriers corresponding to both these relative motions have been calculated (Figure 2d) at a QM level. The translational movement is governed by a relatively high energy barrier (ca. 120 kJ/mol) compared to that (70 kJ/mol) associated with the partial circumrotational movement. This difference in energy can be attributed (Figure S7) to the strong steric hindrance in the case of the translational movement, rendering it less favorable, despite the effective interactions between the pyrene moieties of the two cyclophanes since they are not necessarily aligned.

For the most favored motion—namely partial circumrotation—insight into the effective interactions has been analyzed and characterized. NCI analyses provide[32a] visual

https://doi.org/10.1021/jacs.2c10591
J. Am. Chem. Soc. 2022, 144, 23551−23559

information for the location and the nature of different NCIs being either repulsive or attractive. Two superstructures along the energy profile during partial circumrotation (Figure 2d) have been highlighted in Figure 3a and b. In the case of the more stable superstructure (Figure 3a), only attractive NCIs—such as [C−H···π] or [π···π]—are observed. In the case of the less stable superstructure (Figure 3b), both attractive and repulsive interactions have been identified, corresponding, respectively, to [C−H···π] and steric interactions. It is also worth noting that, in both cases, van der Waals interactions are present.

In order to examine the effect of relative coconformational motions on the photophysical properties, the three pyrene-containing compounds, ^{2,7}**PyDB**·2PF$_6$, $^{2,7-2,7}$**PyBox**·4PF$_6$, and $^{2,7-2,7}$**PyHC**·8PF$_6$, were investigated upon changing the temperature. The photoluminescence properties of these compounds have been reported previously[16] in MeCN solutions at room temperature. The $^{2,7-2,7}$**PyHC**·8PF$_6$ shows a broad exciplex emission band, centered on 593 nm, originating from the stacking of the pyrene-based chromophores, while the ^{2,7}**PyDB**·2PF$_6$ and the $^{2,7-2,7}$**PyBox**·4PF$_6$ display monomeric emissions centered, respectively, on 551 and 554 nm. Variable temperature steady-state fluorescence spectroscopy was carried out in MeCN. On increasing the temperature from 15 to 70 °C, minimal decreases in emission for ^{2,7}**PyDB**·2PF$_6$ (Figure 4a) and $^{2,7-2,7}$**PyBox**·4PF$_6$ (Figure 4b) were observed. In contrast, in the case of the homo[2]catenane, $^{2,7-2,7}$**PyHC**·8PF$_6$, the changes (Figure 4c) in emission are dramatic and are manifested in a significant decrease (Figure 4d) in the fluorescence intensity along with a hypsochromic shift of $\Delta\lambda_{max}$ = 13 nm as the temperature is increased. The fluorescence quantum yield (Φ_f) of $^{2,7-2,7}$**PyHC**·8PF$_6$ is 10.7 ± 0.5% at 20 °C and decreases drastically at 70 °C as Φ_f only reaches 4.9 ± 0.5% (Table S1). This phenomenon is also visible with the naked eye which detects a fading of the luminescence. The emission spectrum of $^{2,7-2,7}$**PyHC**·8PF$_6$ increases dramatically in intensity upon freezing in an optical glass of ^{n}PrCN compared to room temperature (Figure S18) under identical exposure and collection conditions, further confirming the role of molecular motion in modulating the emission at higher temperatures. Moreover, these changes have been observed (Figures S8−S11) only in the emission and not in the absorption spectra. Based on the MICE, the difference in the photoluminescence behavior between these compounds is attributed to the relative circumrotational motion of one cyclophane with respect to other in the homo[2]catenane. At low temperatures, the circumrotational rate is slow, leading to a strong exciplex emission, while, when the temperature is increased, the rate becomes faster and the emission decreases as a consequence of nonradiative relaxations.

Variable-temperature transient absorption spectroscopy was performed in MeCN (Figures 5 and S20−S21). The exciplex lifetime shortens from 15.7 ± 0.6 ns at 20 °C to 10.4 ± 0.6 ns at 70 °C, an observation which is consistent with the concomitant drop in emission yield. The corresponding radiative decay rate decreases by 30% over this range, while the nonradiative decay rate increases by 61% (Table S1), leading to a shortening of the exciplex lifetime. The changes in both of these rates are consistent with the disruption of [π···π] stacking at higher temperatures. Variable-temperature time-resolved fluorescence spectroscopy (Figures S22−S27) also shows an emissive intermediate with a 160-ps lifetime preceding exciplex emission that is independent of temperature and similar to the structural relaxation observed in $^{2,7-2,7}$**PyBox**$^{4+}$. This observation suggests

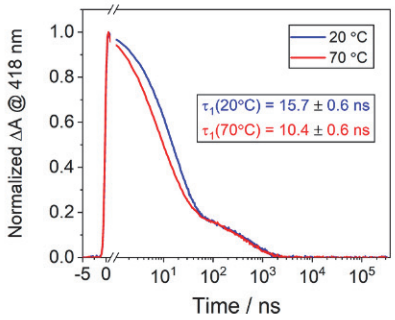

Figure 5. Normalized transient absorption decay at 418 nm for $^{2,7-2,7}$**PyHC**·8PF$_6$in MeCN at 20 °C (blue) and 70 °C (red) following 355 nm excitation.

that the conformational relaxation present over this temperature range does not involve disruption of the [π···π] stacking.

The changes in emission of $^{2,7-2,7}$**PyHC**$^{8+}$ were also investigated in DMF, MeOH, and H_2O solutions.[35] $^{2,7-2,7}$**PyHC**$^{8+}$ exhibits (Figure 6a) solvatochromic behavior,

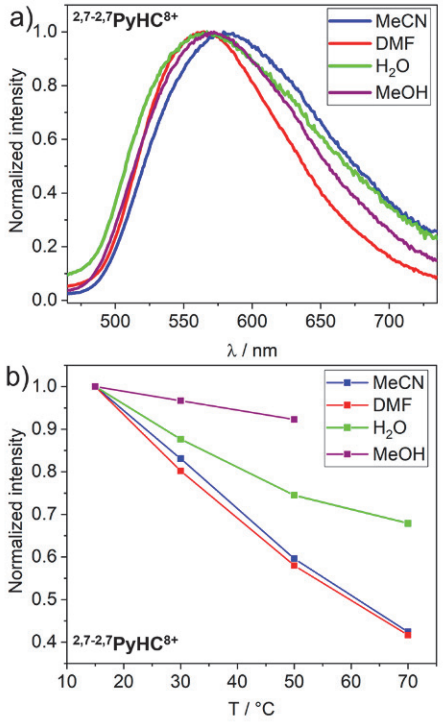

Figure 6. (a) Emission spectra (λ_{exc} = 376 nm) of $^{2,7-2,7}$**PyHC**$^{8+}$ in different solvents, i.e., MeCN (blue), DMF (red), H_2O (green), and MeOH (purple), supporting the presence of solvatochromic behavior. (b) Effect of solvents on the fluorescence of $^{2,7-2,7}$**PyHC**$^{8+}$ as a function of the temperature. These graphs reveal differences in MICE depending on the nature of the solvent.

observed previously[13] for the anthracene-based homo[2]-catenane analogs. At 15 °C, the $^{2,7-2,7}$**PyHC**$^{8+}$ displays exciplex emission, centered on 593, 565, 573, and 567 nm in MeCN, DMF, MeOH, and H_2O, respectively. Upon the progressive heating of the solutions, a decrease of the fluorescence is observed (Figures 6b, S13, S15, and S17) in all four solvents with a clear difference in magnitude. Both MeCN and DMF afford similar rates of decrease, while the changes in H_2O are significantly less evident and in MeOH are almost imperceptible.

https://doi.org/10.1021/jacs.2c10591
J. Am. Chem. Soc. 2022, 144, 23551−23559

The MICE occurring in $^{2,7-2,7}$**PyHC**$^{8+}$ is, therefore, substantially more important in aprotic solvents—such as MeCN and DMF—employing PF_6^- counterions, than it is in protic solvents, such as H_2O and MeOH, using Cl^- counterions. We anticipate that the origin of the MICE disparity results from the existence of [OH···π] interactions between the homo[2]-catenane components (cyclophanes) and the OH groups present in the protic solvents. These interactions affect[36] the solvation energy and the acceleration of the circumrotation rate (k) between the two mechanically interlocked cyclophanes. We note that the increase (Table 1) in k between 293 and 343 K is ca. 10 times lower in MeOH solution to that in DMF. In addition, the counterions, the viscosity of the solvent, and the solubility of the homo[2]catenane in the four solvents might also affect the magnitude of the decrease in fluorescence.

Finally, the reversibility of the temperature-induced changes during emission has been investigated. Upon heating and cooling the homo[2]catenane in MeCN solution, four complete cycles were recorded (Figures 7 and S19). The homo[2]-catenane showed high photothermal stability throughout the cycles since no substantial alteration of the photoluminescence performance was observed. The reversibility of this system is excellent and shows the potential of the mechanical bond and coconformational motion to construct fluorogenic probes and smart photonic devices.

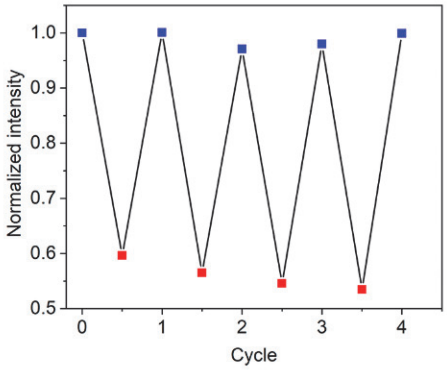

Figure 7. Reversibility of MICE in $^{2,7-2,7}$**PyHC**·8PF_6 in MeCN, (λ_{exc} = 376 nm) at 585 nm upon cooling (25 °C cycles 0, 1, 2, 3, 4) and heating (70 °C cycles 0.5, 1.5, 2.5, 3.5). The reversibility of the system is shown for four complete cycles without observing any significant alteration in the fluorescence.

CONCLUSIONS

An insight into the effect of the coconformational movements of the two mechanically interlocked cyclophanes upon the fluorescence properties of a thermoresponsive homo[2]-catenane—namely $^{2,7-2,7}$**PyHC**$^{8+}$—has been investigated. Analysis of the dynamic behavior by variable-temperature ^{1}H NMR spectroscopy revealed a circumrotational movement involving the cyclophanes of the homo[2]catenane, while a combination of molecular dynamics simulations and quantum mechanics calculations allowed us to gain a better understanding of the importance of translational as well as partial circumrotational movements.

Variable-temperature fluorescence studies highlight a significant temperature-dependent MICE associated with the homo[2]catenane photoluminescence. The MICE characteristics of the catenane are manifested in a remarkable decrease in intensity and a hypsochromic shift of the emission, compared with those exhibited by the cyclophane. The enhanced MICE can be attributed to the additional coconformational motion between the two mechanically interlocked cyclophanes in the homo[2]catenane. In addition, the temperature-induced changes in photoluminescence are reversible for at least four complete cycles. These findings demonstrate the potential of mechanically interlocked molecules to act as efficient temperature probes, thus opening up numerous opportunities in materials sciences and biomedicine.

ASSOCIATED CONTENT

Supporting Information

The Supporting Information is available free of charge at https://pubs.acs.org/doi/10.1021/jacs.2c10591.

Materials, methods and characterization data (NMR, UV−vis and fluorescence spectra), and additional figures for the compounds (PDF)

Video (molecular dynamics and quantum mechanics calculations) (MP4)

AUTHOR INFORMATION

Corresponding Author

J. Fraser Stoddart − *Department of Chemistry, Northwestern University, Evanston, Illinois 60208, United States; School of Chemistry, University of New South Wales, Sydney, NSW 2052, Australia; Stoddart Institute of Molecular Science, Department of Chemistry, Zhejiang University, Hangzhou 310027, China; ZJU-Hangzhou Global Scientific and Technological Innovation Center, Hangzhou 311215, China;* orcid.org/0000-0003-3161-3697; Email: stoddart@northwestern.edu

Authors

Amine Garci − *Department of Chemistry, Northwestern University, Evanston, Illinois 60208, United States*

Arthur H. G. David − *Department of Chemistry, Northwestern University, Evanston, Illinois 60208, United States;* orcid.org/0000-0002-9275-2343

Laura Le Bras − *Laboratoire Chrono-environnement (UMR 6249), Université de Bourgogne Franche-Comté, 25030 Besançon, France*

Marco Ovalle − *Department of Chemistry, Northwestern University, Evanston, Illinois 60208, United States*

Seifallah Abid − *Department of Chemistry, Northwestern University, Evanston, Illinois 60208, United States*

Ryan M. Young − *Department of Chemistry and Institute for Sustainability and Energy at Northwestern, Northwestern University, Evanston, Illinois 60208, United States;* orcid.org/0000-0002-5108-0261

Wenqi Liu − *Department of Chemistry, University of South Florida, Tampa, Florida 33620, United States;* orcid.org/0000-0001-6408-0204

Chandra S. Azad − *Department of Chemistry, Northwestern University, Evanston, Illinois 60208, United States*

Paige J. Brown − *Department of Chemistry and Institute for Sustainability and Energy at Northwestern, Northwestern University, Evanston, Illinois 60208, United States;* orcid.org/0000-0002-2934-0098

Michael R Wasielewski − *Department of Chemistry and Institute for Sustainability and Energy at Northwestern, Northwestern University, Evanston, Illinois 60208, United States;* orcid.org/0000-0003-2920-5440

Complete contact information is available at:
https://pubs.acs.org/10.1021/jacs.2c10591

Author Contributions

[○]A.G. and A.H.G.D. contributed equally to this paper

Notes

The authors declare no competing financial interest.

■ ACKNOWLEDGMENTS

The authors thank Northwestern University for their continued support of this research. The authors acknowledge the Integrated Molecular Structure Education and Research Center (IMSERC) at NU for providing access to equipment for the experiments. L.L.B. would like to thank the supercomputer facilities of the Mésocentre de calcul de Franche-Comté. This project was also supported by the National Science Foundation under Grant Number DMR-2003739 (M.R.W., R.M.Y., P.J.B.). The authors thank Dr. Yuyang Wu for his assistance on VT ^{1}H NMR measurements and Dr. Masoud Kazem-Rostami for helping in taking the pictures with the camera of his mobile phone, of the variable temperature fluorescence experiment performed by A.G.

■ REFERENCES

(1) Michalski, L.; Eckersdorf, K.; Kucharski, J.; McGhee, J. *Temperature Measurement*; Wiley: West Sussex, U.K., 2001.

(2) (a) Zhou, H.; Sharma, M.; Berezin, O.; Zuckerman, D.; Berezin, M. Y. Nanothermometry: From Microscopy to Thermal Treatments. *ChemPhysChem* **2016**, *17*, 27−36. (b) del Rosal, B.; Ximendes, E.; Rocha, U.; Jaque, D. In Vivo Luminescence Nanothermometry: From Materials to Applications. *Adv. Optical Mater.* **2017**, *5*, 1600508. (c) Chen, W. Thermometry and Interpretation of Body Temperature. *Biomed. Eng. Lett.* **2019**, *9*, 3−17. (d) Wang, F.; Han, Y.; Gu, N. Cell Temperature Measurement for Biometabolism Monitoring. *ACS Sens.* **2021**, *6*, 290−302.

(3) (a) Ropelewski, C. F.; Halpert, M. S. North American Precipitation and Temperature Patterns Associated with the El Niño/Southern Oscillation (ENSO). *Mon. Weather Rev.* **1986**, *114*, 2352−2362. (b) Vinnikov, K. Y.; Grody, N. C. Global Warming Trend of Mean Tropospheric Temperature Observed by Satellites. *Science* **2003**, *302*, 269−272. (c) Kawai, Y.; Wada, A. Diurnal Sea Surface Temperature Variation and Its Impact on the Atmosphere and Ocean: A Review. *J. Oceanogr.* **2007**, *63*, 721−744.

(4) (a) Suzuki, H.; Ohno, J. Recent Trends in Temperature Measurement Technology in Iron and Steel Industry. *Trans. Iron Steel Inst. Jpn.* **1979**, *19*, 440−447. (b) Vadivambal, R.; Jayas, D. S. Applications of Thermal Imaging in Agriculture and Food Industry—A Review. *Food Bioprocess Technol.* **2011**, *4*, 186−199. (c) Osornio-Rios, R. A.; Antonino-Daviu, J. A.; Romero-Troncoso, R. D. J. Recent Industrial Applications of Infrared Thermography: A Review. *IEEE Trans. Ind. Inform.* **2019**, *15*, 615−625.

(5) (a) Perruchas, S.; Le Goff, X. F.; Maron, S.; Maurin, I.; Guillen, F.; Garcia, A.; Gacoin, T.; Boilot, J.-P. Mechanochromic and Thermochromic Luminescence of a Copper Iodide Cluster. *J. Am. Chem. Soc.* **2010**, *132*, 10967−10969. (b) Garcia, Y.; Robert, F.; Naik, A. D.; Zhou, G.; Tinant, B.; Robeyns, K.; Michotte, S.; Piraux, L. Spin Transition Charted in a Fluorophore-Tagged Thermochromic Dinuclear Iron(II) Complex. *J. Am. Chem. Soc.* **2011**, *133*, 15850−15853. (c) Pais, V. F.; Lassaletta, J. M.; Fernández, R.; El-Sheshtawy, H. S.; Ros, A.; Pischel, U. Organic Fluorescent Thermometers Based on Borylated Arylisoquinoline Dyes. *Chem.—Eur. J.* **2014**, *20*, 7638−7645. (d) Han, M.; Tian, Y.; Yuan, Z.; Zhu, L.; Ma, B. A Phosphorescent Molecular "Butterfly" that Undergoes a Photoinduced Structural Change allowing Temperature Sensing and White Emission. *Angew. Chem. Int. Ed.* **2014**, *53*, 10908−10912. (e) Vyšniauskas, A.; Qurashi, M.; Gallop, N.; Balaz, M.; Anderson, H. L.; Kuimova, M. K. Unravelling the Effect of Temperature on Viscosity-Sensitive Fluorescent Molecular Rotors. *Chem. Sci.* **2015**, *6*, 5773−5778. (f) Osaki, H.; Chou, C.-M.; Taki, M.; Welke, K.; Yokogawa, D.; Irle, S.; Sato, Y.; Higashiyama, T.; Saito, S.; Fukazawa, A.; Yamaguchi, S. A Macrocyclic Fluorophore Dimer with Flexible Linkers: Bright Excimer Emission with a Long Fluorescence Lifetime. *Angew. Chem. Int. Ed* **2016**, *55*, 7131−7135. (g) Tang, J.-H.; Sun, Y.; Gong, Z.-L.; Li, Z.-Y.; Zhou, Z.; Wang, H.; Li, X.; Saha, M. L.; Zhong, Y.-W.; Stang, P. J. Temperature-Responsive Fluorescent Organoplatinum(II) Metallacycles. *J. Am. Chem. Soc.* **2018**, *140*, 7723−7729. (h) Tang, S.-X.; Wang, N.; Xu, X.-D.; Feng, S. A Ratiometric Fluorescent Thermometer Based on Amphiphilic Alkynylpyrene Derivatives. *New J. Chem.* **2019**, *43*, 6461−6464. (i) Mazza, M. M. A.; Cardano, F.; Cusido, J.; Baker, J. D.; Giordani, S.; Raymo, F. M. Ratiometric Temperature Sensing with Fluorescent Thermochromic Switches. *Chem. Commun.* **2019**, *55*, 1112−1115. (j) Ai, Y.; Chan, M. H.-Y.; Chan, A. K.-W.; Ng, M.; Li, Y.; Yam, V. W.-W. A Platinum(II) Molecular Hinge with Motions Visualized by Phosphorescence Changes. *Proc. Natl. Acad. Sci. U.S.A.* **2019**, *116*, 13856−13861. (k) Ogle, M. M.; McWilliams, A. D. S.; Ware, M. J.; Curley, S. A.; Corr, S. J.; Martí, A. A. Sensing Temperature in Vitro and in Cells Using a BODIPY Molecular Probe. *J. Phys. Chem. B* **2019**, *123*, 7282−7289. (l) Chen, Z.; Tang, J.-H.; Chen, W.; Xu, Y.; Wang, H.; Zhang, Z.; Sepehrpour, H.; Cheng, G.-J.; Li, X.; Wang, P.; Sun, Y.; Stang, P. J. Temperature- and Mechanical-Force-Responsive Self-Assembled Rhomboidal Metallacycle. *Organometallics* **2019**, *38*, 4244−4249. (m) Bardi, B.; Tosi, I.; Faroldi, F.; Baldini, L.; Sansone, F.; Sissa, C.; Terenziani, F. A Calixarene-Based Fluorescent Ratiometric Temperature Probe. *Chem. Commun.* **2019**, *55*, 8098−8101. (n) Keshri, S. K.; Takai, A.; Ishizuka, T.; Kojima, T.; Takeuchi, M. Conformational Dynamics of Monomer versus Dimer-like Features in a Naphthalene-diimide-Based Conjugated Cyclophane. *Angew. Chem. Int. Ed* **2020**, *59*, 5254−5258. (o) Gurskiy, S. I.; Maklakov, S. S.; Dmitrieva, N. E.; Tafeenko, V. A. Effects of Transition Metal Cations and Temperature on the Luminescence of a 3-Cyano-4-dicyanomethylene-5-oxo-4,5-dihydro-1H-pyrrole-2-olate Anion. *New J. Chem.* **2021**, *45*, 21684−21691. (p) Zheng, Y.; Meana, Y.; Mazza, M. M. A.; Baker, J. D.; Minnett, P. J.; Raymo, F. M. Fluorescence Switching for Temperature Sensing in Water. *J. Am. Chem. Soc.* **2022**, *144*, 4759−4763.

(6) (a) Wang, X.-D.; Wolfbeis, O. S.; Meier, R. J. Luminescent Probes and Sensors for Temperature. *Chem. Soc. Rev.* **2013**, *42*, 7834−7869. (b) Ogle, M. M.; Smith McWilliams, A. D.; Jiang, B.; Martí, A. A. Latest Trends in Temperature Sensing by Molecular Probes. *ChemPhotoChem* **2020**, *4*, 255−270.

(7) Su, D.; Teoh, C. L.; Wang, L.; Liu, X.; Chang, Y.-T. Motion-Induced Change in Emission (MICE) for Developing Fluorescent Probes. *Chem. Soc. Rev.* **2017**, *46*, 4833−4844.

(8) (a) Chapman, C. F.; Liu, Y.; Sonek, G. J.; Tromberg, B. J. The Use of Exogenous Fluorescent Probes for Temperature Measurements in Single Living Cells. *Photochem. Photobiol.* **1995**, *62*, 416−425. (b) Bur, A. J.; Vangel, M. G.; Roth, S. C. Fluorescence Based Temperature Measurements and Applications to Real-Time Polymer Processing. *Polym. Eng. Sci.* **2001**, *41*, 1380−1389. (c) Vu, T. T.; Méallet-Renault, R.; Clavier, G.; Trofimov, B. A.; Kuimova, M. K. Tuning BODIPY Molecular Rotors into the Red: Sensitivity to Viscosity *vs.* Temperature. *J. Mater. Chem. C* **2016**, *4*, 2828−2833. (d) Huang, Z.; Li, N.; Zhang, X.; Wang, C.; Xiao, Y. Fixable Molecular Thermometer for Real-Time Visualization and Quantification of Mitochondrial Temperature. *Anal. Chem.* **2018**, *90*, 13953−13959.

(9) (a) Evans, N. H.; Beer, P. D. Progress in the Synthesis and Exploitation of Catenanes since the Millennium. *Chem. Soc. Rev.* **2014**, *43*, 4658−4683. (b) Gil-Ramírez, G.; Leigh, D. A.; Stephens, A. J. Catenanes: Fifty Years of Molecular Links. *Angew. Chem. Int. Ed.* **2015**, *54*, 6110−6150.

(10) Bruns, C. J.; Stoddart, J. F. *The Nature of the Mechanical Bonds: From Molecules to Machines*; John Wiley & Sons: Hoboken, NJ, 2016.

(11) (a) Armaroli, N.; Balzani, V.; Barigelletti, F.; De Cola, L.; Sauvage, J.-P.; Hemmert, C. Excited-State Properties in Supramolecular Systems. Luminescence and Intercomponent Interactions in a 3-Catenand and some 3-Catenates. *J. Am. Chem. Soc.* **1991**, *113*, 4033−

4035. (b) Hamilton, D. G.; Montalti, M.; Prodi, L.; Fontani, M.; Zanello, P.; Sanders, J. K. M. Photophysical and Electrochemical Characterisation of the Interactions between Components in Neutral π-Associated [2]Catenanes. *Chem.—Eur. J.* **2000**, *6*, 608−617. (c) Blanco, V.; García, M. D.; Peinador, C.; Quintela, J. M. Self-assembly of New Fluorescent Pd(II) and Pt(II) 2,7-Diazapyrenium-Based Metallocycles and Study of their Inclusion Complexes and [3]Catenanes. *Chem. Sci.* **2011**, *2*, 2407−2416. (d) Lee, J.-J.; Baumes, J. M.; Connell, R. D.; Oliver, A. G.; Smith, B. D. Squaraine [2]Catenanes: Synthesis, Structure and Molecular Dynamics. *Chem. Commun.* **2011**, *47*, 7188−7190. (e) Dekhtiarenko, M.; Pascal, S.; Elhabiri, M.; Mazan, V.; Canevet, D.; Allain, M.; Carré, V.; Aubriet, F.; Voitenko, Z.; Sallé, M.; Siri, O.; Goeb, S. Reversible pH-Controlled Catenation of a Benzobisimidazole-Based Tetranuclear Rectangle. *Chem.—Eur. J.* **2021**, *27*, 15922−15927. (f) Yang, S.; Zhao, C.-X.; Crespi, S.; Li, X.; Zhang, Q.; Zhang, Z.-Y.; Mei, J.; Tian, H.; Qu, D.-H. Reversibly Modulating a Conformation-Adaptive Fluorophore in [2]Catenane. *Chem* **2021**, *7*, 1544−1556. (g) Wang, Y.; Lu, S.; Wang, X.-Q.; Niu, Y.-F.; Wang, H.; Wang, W. Synthesis, Structure Elucidation and Functionalization of Sulfonamide [2]Catenanes. *Org. Chem. Front* **2021**, *8*, 4994−5001. (h) Deng, Y.; Lai, S. K.-M.; Kong, L.; Au-Yeung, H. Y. Fine-Tuning of the Optical Output in a Dual Responsive Catenane Switch. *Chem. Commun.* **2021**, *57*, 2931−2934.

(12) Barendt, T. A.; Ferreira, L.; Marques, I.; Félix, V.; Beer, P. D. Anion- and Solvent-Induced Rotary Dynamics and Sensing in a Perylene Diimide [3]Catenane. *J. Am. Chem. Soc.* **2017**, *139*, 9026−9037.

(13) Garci, A.; Beldjoudi, Y.; Kodaimati, M. S.; Hornick, J. E.; Nguyen, M. T.; Cetin, M. M.; Stern, C. L.; Roy, I.; Weiss, E. A.; Stoddart, J. F. Mechanical-Bond-Induced Exciplex Fluorescence in an Anthracene-Based Homo[2]catenane. *J. Am. Chem. Soc.* **2020**, *142*, 7956−7967.

(14) (a) Gong, X.; Young, R. M.; Hartlieb, K. J.; Miller, C.; Wu, Y.; Xiao, H.; Li, P.; Hafezi, N.; Zhou, J.; Ma, L.; Cheng, T.; Goddard, W. A., III; Farha, O. K.; Hupp, J. T.; Wasielewski, M. R.; Stoddart, J. F. Intramolecular Energy and Electron Transfer Within a Diazaperopyrenium-Based Cyclophane. *J. Am. Chem. Soc.* **2017**, *139*, 4107−4116. (b) Roy, I.; Bobbala, S.; Zhou, J.; Nguyen, M. T.; Nalluri, S. K. M.; Wu, Y.; Ferris, D. P.; Scott, A. E.; Wasielewski, M. R.; Stoddart, J. F. ExTzBox: A Glowing Cyclophane for Live Cell Imaging. *J. Am. Chem. Soc.* **2018**, *140*, 7206−7212. (c) Cetin, M. M.; Beldjoudi, Y.; Roy, I.; Anamimoghadam, O.; Bae, Y. J.; Young, R. M.; Krzyaniak, M. D.; Stern, C. L.; Philp, D.; Alsubaie, F. M.; Wasielewski, M. R.; Stoddart, J. F. Combining Intra- and Intermolecular Charge Transfer with Polycationic Cyclophanes to Design 2D Tessellations. *J. Am. Chem. Soc.* **2019**, *141*, 18727−18739. (d) Garci, A.; Abid, S.; David, A. H. G.; Codesal, M. D.; Đorđević, L.; Young, R. M.; Sai, H.; Le Bras, L.; Perrier, A.; Ovalle, M.; Brown, P. J.; Stern, C. L.; Campaña, A. G.; Stupp, S. I.; Wasielewski, M. R.; Blanco, V.; Stoddart, J. F. Aggregation Induced Emission and Circularly Polarized Luminescence Duality in Tetracationic Binaphthyl-Based Cyclophanes. *Angew. Chem. Int. Ed.* **2022**, *61*, No. e202208679.

(15) Roy, I.; David, A. H. G.; Das, P. J.; Pe, D. J.; Stoddart, J. F. Fluorescent Cyclophanes and Their Applications. *Chem. Soc. Rev.* **2022**, *51*, 5557−5605.

(16) Garci, A.; Weber, J. A.; Young, R. M.; Kazem-Rostami, M.; Ovalle, M.; Beldjoudi, Y.; Atilgan, A.; Bae, Y. J.; Liu, W.; Jones, L. O.; Stern, C. L.; Schatz, G. C.; Farha, O. K.; Wasielewski, M. R.; Stoddart, J. F. Mechanically Interlocked Pyrene-Based Photocatalysts. *Nat. Catal* **2022**, *5*, 524−533.

(17) Gong, X.; Zhou, J.; Hartlieb, K. J.; Miller, C.; Li, P.; Farha, O. K.; Hupp, J. T.; Young, R. M.; Wasielewski, M. R.; Stoddart, J. F. Toward a Charged Homo[2]catenane Employing Diazapyenium Homophilic Recognition. *J. Am. Chem. Soc.* **2018**, *140*, 6540−6544.

(18) (a) Ashton, P. R.; Goodnow, T. T.; Kaifer, A. E.; Reddington, M. V.; Slawin, A. M. Z.; Spencer, N.; Stoddart, J. F.; Vicent, C.; Williams, D. J. A [2]Catenane Made to Order. *Angew. Chem., Int. Ed. Engl.* **1989**, *28*, 1396−1399. (b) Leigh, D. A.; Murphy, A.; Smart, J. P.; Deleuze, M. S.; Zerbetto, F. Controlling the Frequency of Macrocyclic Ring Rotation in Benzylic Amide [2]Catenanes. *J. Am. Chem. Soc.* **1998**, *120*, 6458−6467. (c) Deleuze, M. S.; Leigh, D. A.; Zerbetto, F. How Do Benzylic Amide [2]Catenane Rings Rotate? *J. Am. Chem. Soc.* **1999**, *121*, 2364−2379. (d) Miljanić, O. Š.; Dichtel, W. R.; Khan, S. I.; Mortezaei, S.; Heath, J. R.; Stoddart, J. F. Structural and Co-Conformational Effects of Alkyne-Derived Subunits in Charged Donor-Acceptor [2]Catenanes. *J. Am. Chem. Soc.* **2007**, *129*, 8236−8246. (e) Fang, L.; Basu, S.; Sue, C.-H.; Fahrenbach, A. C.; Stoddart, J. F. Syntheses and Dynamics of Donor-Acceptor [2]Catenanes in Water. *J. Am. Chem. Soc.* **2011**, *133*, 396−399. (f) Marrs, C. N.; Evans, N. H. The Rapid Synthesis and Dynamic Behaviour of an Isophthalamide [2]Catenane. *Org. Biomol. Chem.* **2015**, *13*, 11021−11025. (g) Fernando, I. R.; Frasconi, M.; Wu, Y.; Liu, W.-G.; Wasielewski, M. R.; Goddard, W. A., III; Stoddart, J. F. Sliding−Ring Catenanes. *J. Am. Chem. Soc.* **2016**, *138*, 10214−10225. (h) Segawa, Y.; Kuwayama, M.; Hijikata, Y.; Fushimi, M.; Nishihara, T.; Pirillo, J.; Shirasaki, J.; Kubota, N.; Itami, K. Topological Molecular Nanocarbons: All-Benzene Catenane and Trefoil Knot. *Science* **2019**, *365*, 272−276. (i) Ng, A. W. H.; Lai, S. K.-M.; Yee, C.-C.; Au-Yeung, H. Y. Macrocycle Dynamics in a Branched [8]Catenane Controlled by Three Different Stimuli in Three Different Regions. *Angew. Chem. Int. Ed.* **2022**, *61*, e202110200.

(19) Ma, Y.; Centola, M.; Keppner, D.; Famulok, M. Interlocked DNA Nanojoints for Reversible Thermal Sensing. *Angew. Chem. Int. Ed.* **2020**, *59*, 12455−12459.

(20) Pérez, N. H.; Sherin, P. S.; Posligua, V.; Greenfield, J. L.; Fuchter, M. J.; Jelfs, K. E.; Kuimova, M. K.; Lewis, J. E. M. Emerging Properties from Mechanical Tethering Within a Post-Synthetically Functionalised Catenane Scaffold. *Chem. Sci.* **2022**, *13*, 11368−11375.

(21) Abraham, M. J.; Murtola, T.; Schulz, R.; Páll, S.; Smith, J. C.; Hess, B.; Lindahl, E. GROMACS: High Performance Molecular Simulations Through Mult-Level Parallelism from Laptops to Supercomputers. *SoftwareX* **2015**, *1−2*, 19−25.

(22) Wang, J.; Wolf, R. M.; Caldwell, J. W.; Kollman, P. A.; Case, D. A. Development and Testing of a General AMBER Force Field. *J. Comput. Chem.* **2004**, *25*, 1157−1174.

(23) (a) Wang, J.; Wang, W.; Kollman, P. A.; Case, D. A. Automatic Atom Type and Bond Type Perception in Molecular Mechanical Calculations. *J. Mol. Graph* **2006**, *25*, 247−260. (b) Batista, P. R.; Wilter, A.; Durham, E. H. A. B.; Pascutti, P. G. Molecular Dynamics Simulation Applied to the Study of Subtypes of HIV-1 Protease Common to Brazil, Africa, and Asia. *Cell Biochem. Biophys.* **2006**, *44*, 395−404.

(24) (a) Darden, T.; York, D.; Pedersen, L. Particle Mesh Ewald: An N log(N) Method for Ewald Sums in Large Systems. *J. Chem. Phys.* **1993**, *98*, 10089−10092. (b) Essmann, U.; Perera, L.; Berkowitz, M. L.; Darden, T.; Lee, H.; Pedersen, L. G. A Smooth Particle Mesh Ewald Method. *J. Chem. Phys.* **1995**, *103*, 8577−8593.

(25) Berendsen, H. J. C.; Postma, J. P. M.; van Gunsteren, W. F.; DiNola, A.; Haak, J. R. Molecular Dynamics with Coupling to an External Bath. *J. Chem. Phys.* **1984**, *81*, 3684−3690.

(26) (a) Nosé, S.; Klein, M. Constant Pressure Molecular Dynamics for Molecular Systems. *Mol. Phys.* **1983**, *50*, 1055−1076. (b) Nosé, S. A. Unified Formulation of the Constant Temperature Molecular Dynamics Methods. *J. Chem. Phys.* **1984**, *81*, 511−519. (c) Hoover, W. G. Canonical Dynamics: Equilibrium Phase-Space Distributions. *Phys. Rev. A* **1985**, *31*, 1695−1697.

(27) Parrinello, M.; Rahman, A. Polymorphic Transitions in Single Crystals: A New Molecular Dynamics Method. *J. Appl. Phys.* **1981**, *52*, 7182−7190.

(28) Frisch, M. J.; Trucks, G. W.; Schlegel, H. B.; Scuseria, G. E.; Robb, M. A.; Cheeseman, J. R.; Scalmani, G.; Barone, V.; Petersson, G. A.; Nakatsuji, H.; Li, X.; Caricato, M.; Marenich, A.; Bloino, J.; Janesko, B. G.; Gomperts, R.; Mennucci, B.; Hratchian, H. P.; Ortiz, J. V.; Izmaylov, A. F.; Sonnenberg, J. L.; Williams-Young, D.; Ding, F.; Lipparini, F.; Egidi, F.; Goings, J.; Peng, B.; Petrone, A.; Henderson, T.; Ranasinghe, D.; Zakrzewski, V. G.; Gao, J.; Rega, N.; Zheng, G.; Liang, W.; Hada, M.; Ehara, M.; Toyota, K.; Fukuda, R.; Hasegawa, J.; Ishida, M.; Nakajima, T.; Honda, Y.; Kitao, O.; Nakai, H.; Vreven, T.; Throssell, K.; Montgomery, J. A., Jr.; Peralta, J. E.; Ogliaro, F.; Bearpark, M.; Heyd, J. J.; Brothers, E.; Kudin, K. N.; Staroverov, V. N.; Keith, T.;

https://doi.org/10.1021/jacs.2c10591
J. Am. Chem. Soc. 2022, 144, 23551−23559

Kobayashi, R.; Normand, J.; Raghavachari, K.; Rendell, A.; Burant, J. C.; Iyengar, S. S.; Tomasi, J.; Cossi, M.; Millam, J. M.; Klene, M.; Adamo, C.; Cammi, R.; Ochterski, J. W.; Martin, R. L.; Morokuma, K.; Farkas, O.; Foresman, J. B.; Fox, D. J. *Gaussian 09*, Revision C.01; Gaussian, Inc., Wallingford, CT, 2016.

(29) Chai, J.-D.; Head-Gordon, M. Long-Range Corrected Hybrid Density Functionals with Damped Atom-Atom Dispersion Corrections. *Phys. Chem. Chem. Phys.* **2008**, *10*, 6615−6620.

(30) Le Bras, L.; Dory, Y. L.; Champagne, B. Computational Prediction of the Supramolecular Self-Assembling Properties of Organic Molecules: The Role of Conformational Flexibility of Amide Moieties. *Phys. Chem. Chem. Phys.* **2021**, *23*, 20453−20465.

(31) Tomasi, J.; Mennucci, B.; Cammi, R. Quantum Mechanical Continuum Solvation Models. *Chem. Rev.* **2005**, *105*, 2999−3094.

(32) (a) Johnson, E. R.; Keinan, S.; Mori-Sánchez, P.; Contreras-García, J.; Cohen, A. J.; Yang, W. Revealing Noncovalent Interactions. *J. Am. Chem. Soc.* **2010**, *132*, 6498−6506. (b) Contreras-García, J.; Johnson, E. R.; Keinan, S.; Chaudret, R.; Piquemal, J.-P.; Beratan, D. N.; Yang, W. NCIPLOT: A Program for Plotting Noncovalent Interactions Regions. *J. Chem. Theory Comput.* **2011**, *7*, 625−632.

(33) Young, R. M.; Dyar, S. M.; Barnes, J. C.; Juríček, M.; Stoddart, J. F.; Co, D. T.; Wasielewski, M. R. Ultrafast Conformational Dynamics of Electron Transfer in $ExBox^{4+}$⊂Perylene. *J. Phys. Chem. A* **2013**, *117*, 12438−12448.

(34) Juríček, M.; Strutt, N. L.; Barnes, J. C.; Butterfield, A. M.; Dale, E. J.; Baldridge, K. K.; Stoddart, J. F.; Siegel, J. S. Induced-Fit Catalysis of Corannulene Bowl-to-Bowl Inversion. *Nat. Chem.* **2014**, *6*, 222−228.

(35) Measurements in MeCN and DMF were performed with $^{2,7-2,7}$**PyHC**·8PF_6, while, in MeOH and H_2O, $^{2,7-2,7}$**PyHC**·8Cl was employed.

(36) Maier, J. M.; Li, P.; Vik, E. C.; Yehl, C. J.; Strickland, S. M. S.; Shimizu, K. D. Measurement of Solvent OH−π Interactions Using a Molecular Balance. *J. Am. Chem. Soc.* **2017**, *139*, 6550−6553.

https://doi.org/10.1021/jacs.2c10591
J. Am. Chem. Soc. 2022, 144, 23551−23559